Bovine pericardium of high fibre dispersion has high fatigue life and increased collagen content; potentially an untapped source of heart valve leaflet tissue

Alix Whelan[1,2,3], Elizabeth Williams[1,2], David Nolan[1,2], Bruce Murphy [1,2,4], Paul Gunning[5], David O'Reilly[3], Caitríona Lally[1,2,4*]

[1] Trinity Centre for Bioengineering, Trinity Biomedical Sciences Institute, Trinity College Dublin, Dublin 2, Ireland

[2] Department of Mechanical and Manufacturing Engineering, School of Engineering, Trinity College Dublin, Dublin 2, Ireland

[3] Structural Heart Division, Boston Scientific Corporation, Galway, Ireland

[4] Advanced Materials and Bioengineering Research Centre (AMBER), Royal College of Surgeons in Ireland and Trinity College Dublin, Dublin, Ireland

[5]Structural Heart Division, Boston Scientific Corporation, Los Gatos, CA 95032, USA

Abbreviated title:

Investigation of high fibre dispersion pericardium

*Corresponding author:

Caitriona Lally

Department of Mechanical and Manufacturing Engineering, School of Engineering, Trinity College Dublin, Dublin 2, Ireland

Tel: +353 1896 3159

Fax: +353 1 896 1383

Email address: lallyca@tcd.ie

Abstract

Bioprosthetic heart valves (BHVs) are implanted in aortic valve stenosis patients to replace the native, dysfunctional valve. Yet, the long-term performance of the glutaraldehyde-fixed bovine pericardium (GLBP) leaflets is known to reduce device durability. The aim of this study was to investigate a type of commercial-grade GLBP which has been over-looked in the literature to date; that of high collagen fibre dispersion (HD). Under uniaxial cyclic loading conditions, it was observed that the fatigue behaviour of HD GLBP was substantially equivalent to GLBP in which the fibres are highly aligned along the loading direction. It was also found that HD GLBP had a statistically significant 9.5% higher collagen content when compared to GLBP with highly aligned collagen fibres. The variability in diseased BHV delivery sites results in unpredictable and complex loading patterns across leaflets *in vivo.* This study presents the possibility of a shift from the traditional choice of circumferentially aligned GLBP leaflets, to that of high fibre dispersion arrangements. Characterised by its high fatigue life and increased collagen content, in addition to multiple fibre orientations, GLBP of high fibre dispersion may provide better patient outcomes under the multi-directional loading to which BHV leaflets are subjected *in vivo.*

Key terms: collagen content, collagen architecture, uniaxial tension, cyclic loading

Nomenclature

AS	Aortic valve stenosis	*PD*	Preferred fibre direction
BHV	Bioprosthetic heart valve	*SALS*	Small angle light scattering
GLBP	Glutaraldehyde-fixed bovine pericardium	*SHG*	Second harmonic generation
HA	Highly aligned fibres	*TAVR*	Transcatheter aortic valve replacement
HD	High fibre dispersion	*XD*	Cross fibre direction

1. Introduction

Aortic valve stenosis (AS) is the narrowing of the aortic valve orifice, causing a restriction in blood flow through the valvular area. It is estimated that 12.4% of the US population over the age of 75 suffer from AS [24]. Without intervention, the patient survival rate is approximately 20% at 5 years post-diagnosis [20].

Bioprosthetic heart valves (BHVs) are delivered to the aortic valve orifice to replace the patient's native dysfunctional valve, via transcatheter aortic valve replacement (TAVR) procedure techniques. These devices typically consist of a metallic frame, to which leaflets made from pericardial tissue are attached. Glutaraldehyde-fixed bovine pericardium (GLBP) is employed in 6 of 9 CE-marked patient BHV devices, and is the material chosen for this study [27].

The long-term durability of BHV devices is understood to be inadequate, with numerous clinical reports of premature device failure. Both calcification and tears have been observed on clinically explanted valves; the two primary failure modes for tissue

leaflets *in vivo* [3,12,30,34,35,38,39,50]*.* It is understood that tears occur in regions of high mechanical stress, while the calcification of the tissue is attributed to its previous glutaraldehyde treatment, acting as a catalyst for the accumulation of calcification.

Collagen fibres are the major load bearing component of GLBP, and as such the arrangement of the collagen fibres will govern the mechanical response of the tissue under load. We have shown in our previous work that the fibre alignment in addition to the fibre orientation is a critical factor in determining the ultimate tensile strength and stiffness of commercial GLBP [48]. Although GLBP is employed in a wide variety of clinical treatments, the most popular use is in BHV leaflets, where the leaflets are responsible for controlling blood efflux from the heart with each cardiac cycle. As such, they are subjected to constant cyclic loading *in vivo.* The leaflets experience a complex, multi-directional loading pattern with each cycle, of which there are approximately 60 - 100 per minute [17]**.** It is also important to note that it is not mandatory to pre-screen or characterise collagen fibre architecture in the manufacture of a BHV leaflet, according to ISO 5840 [15].

There is a lack of experimental data available in the literature on the mechanical properties of commercial-grade GLBP. A number of studies report mechanical properties of in-house fixed tissue; i.e. fresh tissue acquired from an abattoir and fixed in-house for 1-7 days [4,9,23,26,28,33,37,44] However, only four of these works pre-sort the tissue according to the mechanically-dominant fibre architecture [23,28,37,44]. Additionally, in-house fixed tissue is vastly different in its mechanical response to commercial-grade tissue, where commercial-grade tissue is fixed for significantly longer time-frames than in-house fixed GLBP. This difference is most evident by comparing stress-strain profiles, see for example; [44] and [48]. A clear limitation of all available experimental data is the inability to subject the tissue to *in vivo* fatigue conditions. The loads exerted upon

the leaflets *in situ* are complex, at extremely high cycle numbers and relatively low frequencies [2,8,16,46]. Specifically, 5 years of *in vivo* operation equates to approximately 200 million cycles. Thus, an experiment to assess leaflet behaviour to 200 million cycles, at a physiological speed of 1.3-1.5 Hz, would take 5 years. However, using elevated frequencies presents its own problems. Accelerated testing speeds can result in non-physiological loading and thus, a non-physiologically relevant response of the tissue. Thus, the most efficient and practical method of assessing the behaviour BHV leaflets *in vivo* is the use of computational models.

To develop a realistic model of the *in vivo* behaviour of BHV leaflets, an accurate GLBP material model is required. There have been many recent advances in modelling the experimentally observed strain induced permanent set of GLBP, as well as the strain-driven damage of fibres in collagenous tissues [11,49]. However, the data in the literature to which current BHV models are calibrated, relates to in-house fixed tissue [21,22,29,31,41,42,49]. Thus, a more complete experimental database and understanding of commercial-grade GLBP is required to improve computational models that will inform future BHV designs.

The current study aims to fill this knowledge gap, and was motivated by the findings of our previous work on commercially-available GLBP; where the ultimate tensile strength and stiffness of specimens with high fibre dispersion were substantially equivalent to those in which the fibres were aligned along the uniaxial load direction [48]. Thus, this study explores the fatigue response of GLBP specimens with high fibre dispersion. To the authors' knowledge, this is the first time that the dynamic response of commercial-grade GLBP with a high fibre dispersion architecture has been reported. For completeness, the fatigue performance of specimens from the same commercial-grade GLBP, with collagen fibres aligned parallel and perpendicular to the loading

direction, is also determined here. Additionally, the collagen content of high fibre dispersion (HD) and highly aligned (HA) GLBP specimens were analysed to investigate any differences between specimen groups.

The complex loading observed across leaflets *in vivo* [2,8,16,46] motivates the exploration of high fibre dispersion GLBP, as it is hypothesized that leaflets characterised by a multi-orientated fibre architecture would be better suited to withstanding this multi-directional loading regime. Importantly, patients receiving BHV devices typically present with non-circular valve orifices due to the stenosing of the valvular site [13]. Consequently, the loading on the device is heterogeneous and varies from patient-to-patient. Thus, the use of a GLBP leaflet with fibres highly aligned in a single direction could result in areas with a paucity of fibres aligned to the localised principal loading direction. However, employment of leaflets with highly dispersed fibres are structurally more suited to these unpredictable and patient-specific loading directions, due to their characteristic multi-directional fibre organisation.

2. Materials & Methods:

2.1. Sample preparation and Small angle light scattering analysis

Commercial-grade GLBP was obtained from Boston Scientific Corporation (Galway, Ireland). This GLBP tissue was manufactured in a process analogous to the GLBP used in commercial devices. As this tissue was not used in patient devices, however, it is referred to in this work as commercial-grade GLBP. The primary difference between commercial-grade GLBP and 'in-house' fixed tissue is the glutaraldehyde exposure time, which is an order of magnitude greater for commercial-grade GLBP.

Unlike 'in-house' fixed tissue and commercially available GLBP, this tissue has not been explored previously in the literature [44,48]. The commercial-grade GLBP used in

this study was subjected to controlled loads during glutaraldehyde fixation. In contrast, the commercial tissue used in our previous study was not [48]. As both tissues are fixed under the same conditions otherwise, we also compare the mechanical properties of the commercial-grade GLBP in this study to that of commercial GLBP in our previous study. This comparison serves to investigate any effect of fixation load on the subsequent mechanical properties of GLBP, once it has been suitably fixed for an extended time period.

Small angle light scattering (SALS) was used to non-destructively quantify the fibre architecture of dogbone specimens (gauge length 12.5mm and gauge width 2.27 mm) harvested from full commercial-grade GLBP patches. SALS is a long-established non-destructive, optical technique in which a laser beam is passed through the tissue, and the resulting scattered light distribution is used to measure both dominant fibre orientation and alignment [32]. The specific system and scanning parameters chosen here were the same as our previous work [10,48].

A custom Matlab code (The Mathworks, Inc., MA, United States) analyses the images to calculate the dominant fibre angle and alignment of each specimen, which is measured as an eccentricity value. Eccentricity (i.e. alignment) values typically range from 0.5 to 0.9, indicating low to high alignment, respectively. The results are presented as a contour plot, as seen in Figure 1.

Table 1 summarises the specimen classification criteria for the three groups in this study: cross-fibre specimens (XD), high fibre dispersion specimens (HD) and preferred fibre (PD) specimens. Note: The angle for the HD group is listed as ‘N/A’ to emphasise the absence of a dominant fibre angle for this specimen group. Although a mean angle was calculated for these specimens in the Matlab post-processing of SALS images, it

is not presented here so that this sample group is interpreted as specimens with a very low level of fibre alignment and no dominant fibre angle. As such, HD samples are loaded uniaxially, along the dogbone gauge length, irrespective of the measured mean fibre angle. These samples are classified as having fibre dispersion above a threshold that the fibre angle is not mechanically significant.

After conducting an initial regional SALS analysis on a full GLBP patch (9 x 16 cm), dogbone specimens are cut from specific regions identified as having high fibre alignment (for XD, PD samples) or high fibre dispersion (HD samples). All dogbone specimens are then analysed again across a 6 x 1 mm region (at 250 µm increments; 96 images per specimen), to ensure they meet the fibre-group specifications as outlined in Table 1. Only specimens which meet the individual XD, HD or PD fibre architecture criteria are selected for uniaxial mechanical testing.

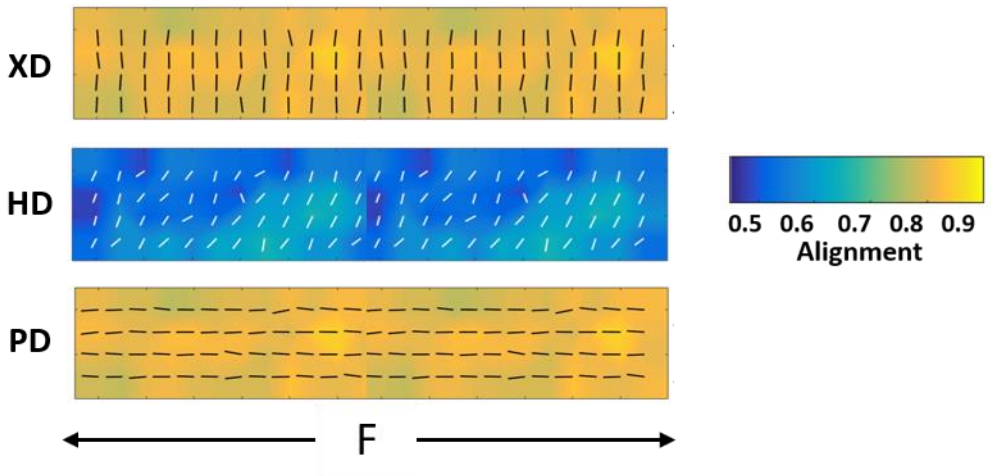

Figure 1: *Representative SALS contour plots for one specimen from the three groups (XD, HD, PD). Colour indicates alignment (low to high; 0.5 to 0.9). White and black vectors indicate fibre angles at each location across region of analysis (6 mm x 1 mm).*

Table 1: Specimen grouping classification. (* Angle is given with respect to loading direction)

Specimen Group	Mean Angle (°) *	Alignment
XD	90 ± 15 °	≥ 0.70
HD	N/A	≤ 0.65
PD	0 ± 15 °	≥ 0.70

2.2. Uniaxial Tensile Cyclic Loading

A total of seven (*n=7)* dogbone specimens for each category (XD, HD, PD) were tested in a Tytron™ Microforce Testing System (MTS Systems Corporation, MN, USA). Each specimen was preconditioned for 1 cycle at 0.01 Hz, at a peak stress of 3 MPa, and then repeatedly cycled at 1.5 Hz at the same peak stress of 3 MPa (with an R-ratio of 0.1). As the maximum operating frequency of the Tytron™ Microforce Testing System for force-controlled tests was 1.5 Hz, a supraphysiological load of 3 MPa was chosen for testing. This load was chosen to accumulate damage in the tissue in a feasible time frame, and also allow for divergences according to fibre architecture to be detected (see Table 1). From our previous work, the ultimate tensile strength of the weakest specimen category (XD), was 4 MPa [48]. Thus, a load of 3 MPa was deemed suitably high to conduct experiments in a realistic time frame, without instant tensile failure of the XD group. Moreover, a 3 MPa load ensures the specimens are loaded to the collagen fibre-dominant region of the stress-strain response (i.e. stiffened linear region), where lower loads would result in a tissue matrix-dominant response (i.e. in

the initial stage of the stress-strain profile). Additionally, computational studies have reported leaflet stresses in the region of 1- 3 MPa [1,21].

The test end-point was defined as run-out at 1 million cycles, or failure. Testing was conducted in a saline bath at 37 °C, to simulate the physiological environment.

2.3. Second Harmonic Generation Imaging (SHG)

Multiphoton imaging (Second Harmonic Generation, or SHG) was employed to visualise the collagen fibre architecture of GLBP in a non-destructive manner. There are two primary differences between the SALS and SHG optical tools utilised in this study. Firstly, SALS is a transmissive technique, while SHG is layer specific and subject to depth limitations (approximately 100 μm for GLBP in the authors' experience). Secondly, SALS records a scattered light image, while SHG permits direct visualisation of the collagen fibre structure. Thus, in this study SALS was used to measure the collagen fibre orientation and alignment as it detects the dominant fibre structure through the tissue thickness, while SHG was used only to visualise the collagen fibres for collagen content analysis.

The purpose of SHG analysis was to determine any differences in the collagen content of highly aligned (i.e. HA) and high fibre dispersion samples (i.e. HD). As commercial-grade GLBP cannot be readily digested down using typical techniques for biochemical assays, SHG was employed as a non-destructive alternative method for measuring collagen content. SHG was used to compare the collagen content between the two specimen categories (i.e. HD and HA), permitted through the application of the same SHG imaging and post-processing parameters for all specimens.

Representative specimens (*n=3)* were chosen from the HD group and the HA groups for image analysis, which was conducted using second harmonic generation (SHG) imaging. As XD/PD specimens meet the same alignment specification, these groups were combined into a 'highly aligned', or HA specimen category. SHG analysis was conducted from both the fibrous and serous face of the GLBP tissue samples, with a Carl Zeiss 710 NLO Microscope (Carl Zeiss, Jena, Germany). This technique involves passing a high energy laser through the sample, and generating a second harmonic of that light. Imposing an incident beam of 840 nm, from a Coherent Chameleon II tuneable laser, generated a second harmonic at the appropriate wavelength to permit collagen visualisation (420 nm). The second harmonic was detected via non-descanned detectors, with a 485 nm short pass emission filter. A W Plan-Apochromat objective was employed, at a magnification of 20X. A z-stack of approximately 20 slices at the centre of each specimen was recorded, with an inter-slice spacing of 8 µm.

2.4. Collagen content analysis

The collagen content of each specimen was calculated using custom-made ImageJ (Maryland, United States) and Matlab (The Mathworks, Inc., MA, United States) programs. A total of twelve measurements were taken for each specimen, which was achieved by calculating the percentage collagen content across four tiles and three slices of images (slice thickness was 8 µm). This was completed using the z-stack of images from the serous face, as the fibres here are typically more organised; providing a more consistent signal between z-slices. The same black and white threshold was applied to each SHG image, to convert collagen fibres to white, and non-collagenous areas to black. Collagen content was then measured as the number of collagen fibre pixels, as a percentage of the total number of image pixels. This method is similar to

that reported by Sulejmani and co-authors [41]. As the fibre arrangement in GLBP changes through the thickness, the slices chosen for analysis were at least 30 μm from the tissue surface. The analysis region for each specimen was 850 μm x 850 μm (across three slices through the depth). Finally, the 36 measurements per group (n=3, at 12 measurements, see above) were analysed with a Student's t-test at a 95% confidence interval.

2.5. Statistical Analysis

Statistical analysis was performed with Prism 6 statistical software (GraphPad Software Inc., San Diego, California). For the cyclic experimental data, a one-way analysis of variance (ANOVA) was performed to investigate statistical significance between each of the three specimen groups (XD, HD, PD). A Tukey's multiple comparisons test was conducted if the ANOVA test result was statistically significant (i.e. $p < 0.05$ for 95% Confidence Interval). As described in section 2.4, collagen content was compared between the HA and HD groups with a Student's t-test, at a 95% confidence interval.

3. Results

3.1. Sample Characterisation

Each of the seven (n=7) specimens chosen for cyclic testing met the alignment and angle (where applicable) requirements for XD, HD and PD specimen groups (see Table 1). The mean and standard deviation of these fibre architecture parameters are summarised in Table 2.

Table 2: Mean angles and alignment values for XD, HD and PD specimens (Uniaxial cyclic loading; see sections 2.1 and 2.2)

Specimen Group	Mean Angle (°)	Alignment
XD (n=7)	84.43 ± 8.76 °	0.75 ± 0.04
HD (n=7)	N/A	0.56 ± 0.03
PD (n=7)	4.74 ± 4.08°	0.76 ± 0.04

3.2. Uniaxial Cyclic Loading

Four (n=4) HD specimens reached run-out at 1 million cycles, in contrast to the XD group whereby four (n=4) samples failed after one cycle (see Figure 2). As in our previous study, each sample in the PD group reached run-out at 1 million cycles [48]. An ANOVA analysis across the three groups (XD, HD, PD) illustrates a statistically significant difference between their fatigue behaviour ($p = 0.0001$). However, a multiple-comparisons analysis reveals no statistically significant difference in the number of cycles completed by HD and PD groups. Furthermore, there was a statistically significant difference in the number of cycles completed between the XD and HD group ($p < 0.01$) and between XD and PD groups ($p < 0.0001$, see figure 2). Full details of collagen fibre angle, alignment and number of cycles completed for each specimen are provided in Appendix A, Table A.1.

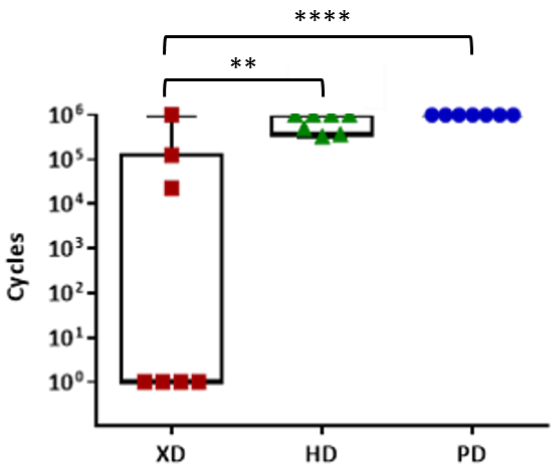

Figure 2: *Cycles completed for XD, HD and PD specimens (**p <0.01, ****p<0.0001).*

Note: No statistically significant difference was found between the HD and PD groups.

3.3. SHG Imaging

SHG imaging of three specimens from each category revealed differences in the fibre architecture between the HD and HA specimen groups. The fibre arrangement of HD specimens appeared wavy and dense (see figure 3 (a-c)). This was in contrast to the HA group, where the fibres appeared comparably to be straighter and more sparse (see figure 3 (d-f)).

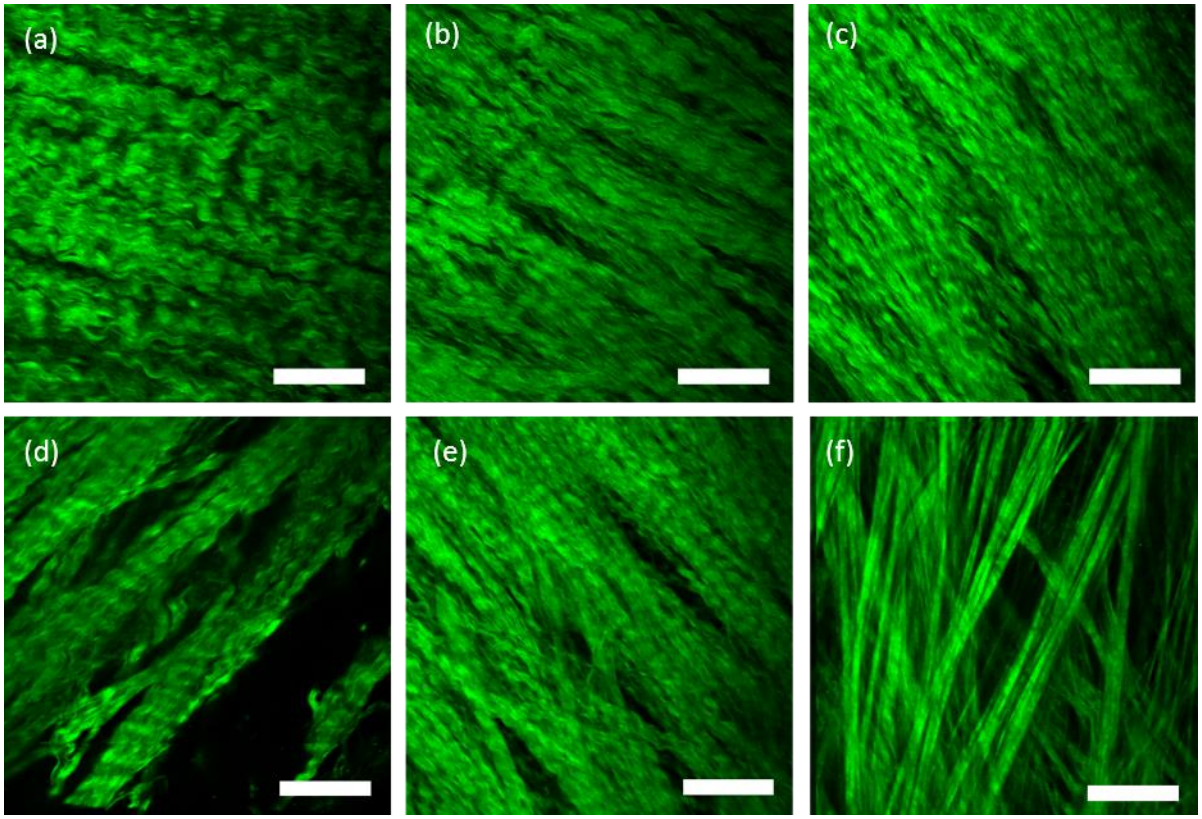

Figure 3: *SHG images of (a-c) HD (high fibre dispersion) specimens and (d-f) HA (highly aligned, i.e. XD/PD) specimens. Scale bar: 100 μm.*

3.4. Collagen content analysis

A statistically significant difference between the alignment values (i.e. level of collagen fibre dispersion) was found between the two specimen groups ($p = 0.0417$, see figure 4). The mean alignment of the HD and HA groups were 0.615 ± 0.0004 and 0.735 ± 0.0002, respectively. The mean collagen content of high fibre dispersion (HD) and highly aligned (HA) specimens was 79.88 ± 0.014% and 72.92 ± 0.017%, respectively.

A student's t-test revealed that the collagen content of the HD group was statistically significantly higher than that of the HA group; where $p = 0.0023$.

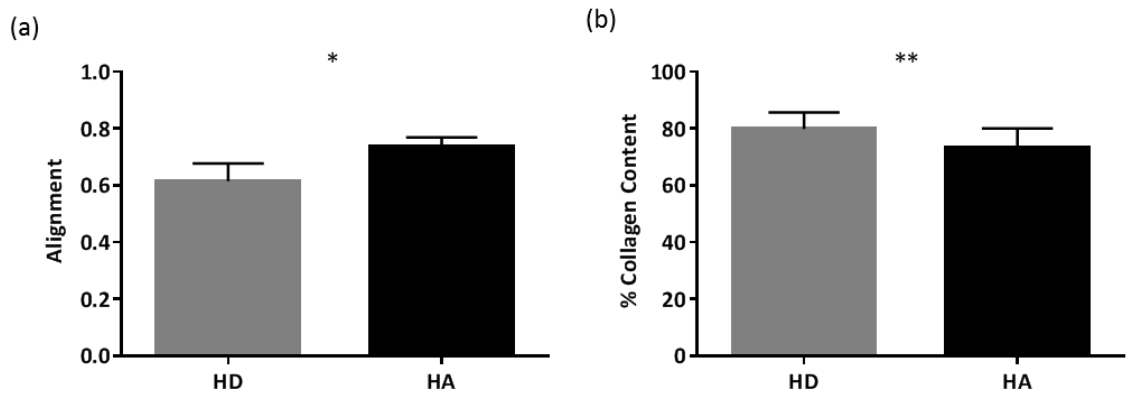

Figure 4: *(a) Alignment values for HD and HA (i.e. XD/PD) groups, according to SALS analysis (see section 2.1), (b) Percentage collagen content of HD and HA groups, according to SHG image analysis (see sections 2.3 and 2.4)*

To illustrate the variability in collagen fibre arrangement across a full patch of GLBP tissue, a SALS analysis of a 9 cm x 16 cm patch of pericardial tissue is included below (see Figure 5). The patch was divided into 24 rectangles (2 cm x 3 cm) and each were imaged with SALS across a 1.8 cm x 2.5 cm region of analysis (43, 200 images in total). The result is displayed as a contour plot, according to angle and alignment, as detailed in Section 2.1. This SALS analysis demonstrates that both fibre angle (black vectors) and alignment (yellow - blue) change regionally across a full GLBP patch. It is possible that regions on a GLBP patch map to distinct anatomical locations. However, as it is unknown where the commercial patch is harvested from on the full pericardial sac, it is not possible to locate regions of specific fibre angle and alignment values in a GLBP patch without imaging the collagen fibres. Full details of the mean fibre angle and alignment of the interrogation regions are given in Appendix A, Table A.2 and Figure A.1.

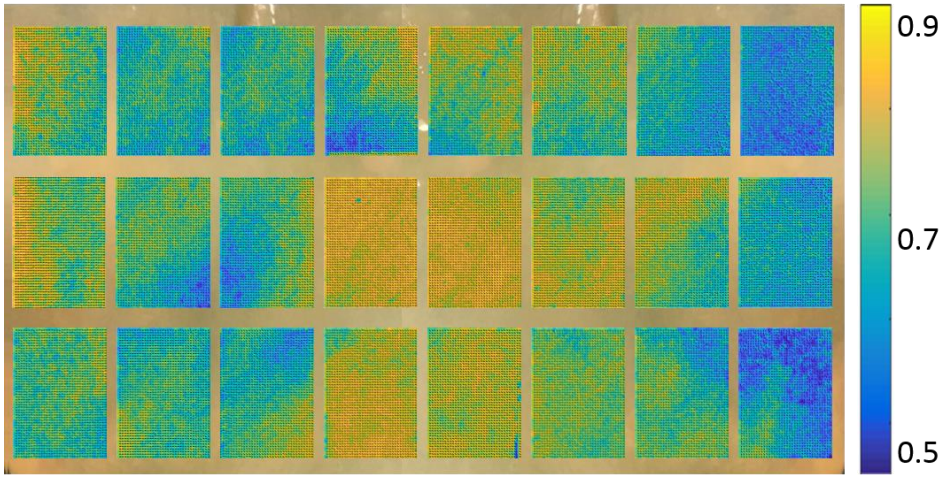

Figure 5: *SALS analysis overlaid on GLBP patch (9 cm x 16 cm), where individual interrogation regions measure 1.8 cm x 2.5 cm. Scale bar on the right indicates collagen fibre alignment, from high to low values (0.9- 0.5, respectively).*

3.5. Fixation technique comparison of two commercial-grade GLBP

To investigate the influence of fixation technique on the mechanical properties of commercial-grade GLBP, the cyclic testing results in this study were retrospectively compared to those of our previous work [48] and are provided in supplementary materials. Additionally, uniaxial static tests to failure were also completed for XD, HD and PD specimens from the tissue in the current study and compared to the results in [48]. This was permitted by the identical mechanical testing protocols in each of the two studies. To the authors' knowledge, this is the first time that the effect of fixation technique has been investigated for commercial-grade GLBP.

The tissue employed in the present study was subjected to controlled loads along its axes during glutaraldehyde treatment. In contrast, the tissue tested in our previous study was not held at specified loads during fixation (Neovasc Inc., British Colombia, Canada). A t-test was employed to investigate the effect of fixation technique on mechanical behaviour. Individual analyses were carried out for each of the specific

fibre architecture categories; XD, HD and PD, where the two tissue types serve as the two groups in the t-test analysis.

T-test analyses revealed no statistically significant differences in the ultimate tensile strength (UTS) or stiffness of XD, HD and PD specimens from the two tissue types (see figure S.1(a,b), in supplementary materials). The UTS is defined as the maximum load the specimen reaches before failure (i.e. the point at which the specimen yields and the stress no longer increases). As observed in the monotonic results, there was no statistically significant difference in the fatigue behaviour of XD and PD specimens from the two different GLBP tissue types (figure S.1(c), in supplementary materials). Note: HD specimens were not tested under dynamic conditions in [48], and thus it is only possible to compare the fatigue behaviour of XD and PD groups between the two tissue types.

Comparison of the static and dynamic behaviour of the specimen groups illustrate that once collagen fibre architecture was quantified prior to testing and specimens were categorised as XD, HD or PD the fixation technique had no statistically significant influence on the mechanical properties of the commercial-grade GLBP.

4. Discussion

This work quantifies the mechanical properties of a different form of GLBP which has not been explored in the literature to-date; i.e. that of HD fibre architecture. The mechanical performance of the HD group demonstrated that specimens with high fibre dispersion are not statistically significantly different to those in which the fibres are highly aligned along the loading direction (see Figure 2). This is the first time the dynamic performance of HD GLBP has been quantified and is especially relevant to the application of bovine pericardium in BHVs, where the leaflets are subjected to

constant cyclic loading *in vivo.* Furthermore, analysis of the fibre angle and alignment of specimens which did not fail due to loading (Appendix 1, Table A.1), and thus could be imaged via SALS post-loading, demonstrated that PD samples became even more aligned towards the load. Additionally, the one XD sample that reached 1 million cycles, reduced in alignment by the test end-point. This indicates that a critical number of fibres were able to re-orientate from the unloaded XD configuration, towards the loading direction to prevent failure. Additionally, the range of mean fibre angles for the HD group (see Table A.1) indicates that beyond a threshold of fibre alignment (< 0.65 in this study), the fibre angle does not solely dictate the tissue behaviour (as it does for XD/PD samples). The absence of a statistically significant difference in the fatigue performance of HD and PD groups indicates that the high fibre dispersion characteristic of the HD group plays a mechanically-significant role, independent of fibre orientation.

To investigate the effect of fixation technique, the UTS and stiffness values of XD, HD and PD specimens harvested from the commercial-grade GLBP used in this study were retrospectively compared to those in [48] (see Supplementary Materials). Additionally, the number of cycles completed by XD and PD groups were compared. Both tissues are commercial-grade GLBP, but were subjected to different loads during glutaraldehyde treatment. T-test analyses illustrated that loading during fixation has no statistically significant effect on the UTS or stiffness of XD, HD and PD specimens when the fibre angle was controlled for by screening the samples with SALS (see Figure S.1(a,b), in supplementary materials). Furthermore, there was no statistically significant difference in the number of cycles completed by XD and PD groups between the two tissue types (see figure S.1(c), in supplementary materials). These results demonstrate that collagen fibre architecture governs the mechanical properties

of GLBP, independent of fixation technique. To the authors' knowledge, this is the first time the effect of load during glutaraldehyde fixation has been investigated for commercial-grade GLBP. It is noteworthy that previous studies in the literature have investigated the mechanical properties of 'in-house' fixed pericardium, which demonstrates increased compliance compared to the commercial-grade pericardium employed in this study [9,23,26,28,33,37,44]. Thus, glutaraldehyde-fixing parameters will alter the mechanical properties of GLBP, but for commercial-grade GLBP tissues, which are exposed to glutaraldehyde for extended time periods, collagen fibre architecture will ultimately govern the mechanical properties.

SHG analysis revealed both a difference in the configuration of fibre bundles and a statistically significant difference in collagen content, between HD and HA groups. HD specimens appeared to have a wavy, dense fibre arrangement. In comparison, the fibre arrangements in HA specimens appeared sparser and straightened (see Figure 3). Furthermore, it is important to note the scale of the SHG images with respect to that of the SALS analysis. Each example SHG image in Figure 3 measures 425 μm x 425 μm, at a localised region at one of multiple 8 μm z-slices through the sample thickness. In contrast, the SALS analysis is conducted through the thickness of the tissue, where each scattered light image (96 per sample) is averaged over the laser beam diameter (128 μm). Additionally, the ≈ 100 μm depth limitation of SHG leaves the central ≈ 200 μm of samples un-accounted for (assuming SHG analysis is conducted from both faces of the tissue). Thus, the mean orientation of an SHG image slice is not representative of the mechanically-dominant fibre structure through the tissue thickness, as measured by SALS.

Moreover, a statistically significant 9.5% higher percentage of collagen content was measured for the HD group in comparison to the HA group (see Figure 4). One might

think that as there are fewer fibres aligned in the direction of loading, that HD specimens would exhibit inferior fatigue behaviour compared to PD specimens. However, this was not the case (see Figure 2). This high fatigue life may be explained by the increased density of fibres in HD specimens compared to PD (see Figure 4), where the net number of collagen fibres in the direction of loading may be similar in each group. Again, this supports the greater suitability of HD GLBP to withstand the multi-directional loading that leaflets experience *in vivo.*

It is clear from Figure 5 that both fibre orientation and alignment vary across a full pericardial patch. Moreover, the location on the pericardial sac from where the patch was extracted is unknown, therefore it is not possible to correlate the axes of the patch with anatomical axial and circumferential orientations. It is clear, however, that there is no global dominant fibre direction in the patch defined by the patch anatomy. Yet, several previous studies have made this assumption in categorising fibre orientation in BP test specimens [5,6,18,45]. It is known that collagen fibres remodel such that they align with principal loading directions [19,37]. In the case of pericardium, it is probable that areas of high fibre dispersion on the full GLBP patch (Figure 5) correlate to anatomical regions on the native pericardial sac that are subjected to multidirectional loading. Furthermore, localised multiple principal loading directions *in vivo* likely requires increased levels of collagen, as seen in Figure 4(b). The SALS analysis of a full patch of commercial-grade GLBP illustrates the importance of pre-screening tissue prior to leaflet harvesting; to avoid extracting leaflets with unsuitable or sub-optimal fibre architectures for *in vivo* loading patterns.

It is known that BHV leaflets are subjected to a number of complex loading patterns and regimes *in vivo* in, where native aortic valve leaflets have a complex fibre architecture [2,7,8,16,46]**.** Furthermore, the delivery sites for TAVR BHV devices are

heterogeneous and vary patient to patient. Aortic valve sites can be circular, elliptical or D-shaped [25,36,43]. The presence of calcification nodules and permanent deformation of the tissue can further exacerbate the divergence of the valvular orifice from a typical or 'ideal' geometry [14,21,40,47]. Ultimately, these diverse sites result in deformation of the BHV metallic frame and atypical leaflet loading patterns that are unpredictable in the manufacturing stage.

It is possible that harvesting leaflets from areas of HD architecture on the pericardial patch will provide improved outcomes, as their multi-orientated fibres may be best suited to withstanding the multi-directional loading to which they are subjected. Exclusive of the suitability of the inherent fibre arrangement of HD tissue to the numerous *in vivo* loading directions, we have also demonstrated the high fatigue life of this tissue type (see Figure 2). Furthermore, we have correlated this fatigue performance to an increased collagen content in comparison to native areas of high fibre alignment (see Figure 4). The combination of fibre architecture, high fatigue life and increased collagen content of HD GLBP presents a possible shift from the current paradigm of optimal leaflet fibre structures. Informally, this is advocated in the literature to be that of a circumferentially aligned BHV leaflet [14,21,40]. Formally, there remains no standardised specification or regulation of leaflet fibre patterns. Consequently, there is no requirement for specific leaflet harvesting sites on a pericardial sac or pre-screening of commercial BHV leaflets[15]. This work presents a possible paradigm shift, to a standardised and controlled definition of optimal BHV leaflet fibre patterns. Employment of a non-destructive optical technique, such as SALS used in this research, would enable routine pre-screening of GLBP patches (see Figure 5) so that leaflet geometries are harvested from mechanically-optimal sites. The results

presented here and in our previous work suggest that this may be from regions of high fibre dispersion, independent of the specific fixing technique used for the leaflet tissue.

It is well documented that currently available BHVs do not meet longevity requirements and must be made increasingly durable [22,31]. Whether this is due to a lack of control over leaflet fibre architectures, or a circumferential arrangement of fibres, HD leaflets present an interesting alternative. Our future work aims to explore the collagen fibre-mediated fatigue behaviour of commercial-grade GLBP, under more complex loading regimes and physiological load levels. This study will provide further insight into the potential use of HD GLBP in commercial BHV leaflets.

Acknowledgements:

The authors would like to thank Brenton Cavanagh (Royal College of Surgeons, Ireland) for his assistance and expertise in conducting the SHG imaging in this study. This research is funded by the Irish Research Council and Boston Scientific Corporation (EBPPG/2016/353).

References:

1. Abbasi, M., and A. N. Azadani. Leaflet stress and strain distributions following incomplete transcatheter aortic valve expansion. *J. Biomech.* 48:3663–3671, 2015.
2. Bouten, C., A. Driessen-Mol, and F. P. T. Baaijens. In situ heart valve tissue engineering: simple devices, smart materials, complex knowledge. *Expert Rev. Med. Devices* 9:453–455, 2012.
3. Butterfield, M., and J. Fisher. Fatigue analysis of clinical bioprosthetic heart valves manufactured using photooxidized bovine pericardium. *J. Heart Valve Dis.* 9:161–6; discussion 167, 2000.
4. Caballero, A., F. Sulejmani, C. Martin, T. Pham, and W. Sun. Evaluation of transcatheter heart valve biomaterials: Biomechanical characterization of bovine and porcine pericardium. *J. Mech. Behav. Biomed. Mater.* 75:486–494, 2017.
5. Choe, J. A., S. Jana, B. J. Tefft, R. S. Hennessy, J. Go, D. Morse, A. Lerman, and M. D. Young. Biomaterial characterization of off-the-shelf decellularized

porcine pericardial tissue for use in prosthetic valvular applications. *J. Tissue Eng. Regen. Med.* 12:1608–1620, 2018.

6. Dalgliesh, A. J., M. Parvizi, C. Noble, and L. G. Griffiths. Effect of cyclic deformation on xenogeneic heart valve biomaterials. *PLoS One* 14:, 2019.

7. Driessen, N. J. B., C. V. C. Bouten, and F. P. T. Baaijens. Improved Prediction of the Collagen Fiber Architecture in the Aortic Heart Valve. *J. Biomech. Eng.* 127:329, 2005.

8. Engelmayr, G. C., D. K. Hildebrand, F. W. . Sutherland, J. E. Mayer, and M. S. Sacks. A novel bioreactor for the dynamic flexural stimulation of tissue engineered heart valve biomaterials. *Biomaterials* 24:2523–2532, 2003.

9. García Páez, J. M., E. Jorge, A. Rocha, M. Maestro, J. L. Castillo-Olivares, I. Millan, A. Carrera, A. Cordon, G. Tellez, and R. Burgos. Mechanical effects of increases in the load applied in uniaxial and biaxial tensile testing: Part I. Calf pericardium. *J. Mater. Sci. Mater. Med.* 13:381–388, 2002.

10. Gaul, R. T., D. R. Nolan, and C. Lally. Collagen fibre characterisation in arterial tissue under load using SALS. *J. Mech. Behav. Biomed. Mater.* 75:359–368, 2017.

11. Ghasemi, M., D. R. Nolan, and C. Lally. An investigation into the role of different constituents in damage accumulation in arterial tissue and constitutive model development. *Biomech. Model. Mechanobiol.* , 2018.doi:10.1007/s10237-018-1054-3

12. Grunkemeier, G. L., H.-H. Li, D. C. Naftel, A. Starr, and S. H. Rahimtoola. Current Problems in Cardiology, Long-term performance of heart valve prostheses. *Curr. Probl. Cardiol.* 25:78–154, 2000.

13. Gunning, P. S., N. Saikrishnan, A. P. Yoganathan, and L. M. McNamara. Total ellipse of the heart valve: the impact of eccentric stent distortion on the regional dynamic deformation of pericardial tissue leaflets of a transcatheter aortic valve replacement. *J. R. Soc. Interface* 12:20150737, 2015.

14. Hart, J. D., G. Cacciola, P. J. . Schreurs, and G. W. . Peters. A three-dimensional analysis of a fibre-reinforced aortic valve prosthesis. *J. Biomech.* 31:629–638, 1998.

15. International Standards Organisation. ISO 5840-3:2013 Cardiovascular implants - cardiac valve prostheses. Part 3: Heart valve substitutes implanted by transcatheter techniques. 2013:104p., 2013.

16. Iyengar, A. K. S., H. Sugimoto, D. B. Smith, and M. S. Sacks. Dynamic In Vitro Quantification of Bioprosthetic Heart Valve Leaflet Motion Using Structured Light Projection. *Ann. Biomed. Eng.* 29:963–973, 2001.

17. James, A. P. Heart rate monitoring using human speech spectral features. *Human-centric Comput. Inf. Sci.* 5:33, 2015.

18. Joyce, K., Y. Rochev, and S. Rahmani. Assessment of the uniaxial experimental parameters utilised for the mechanical testing of bovine pericardium. *J. Mech. Behav. Biomed. Mater.* 96:27–37, 2019.

19. Krasny, W., C. Morin, H. Magoariec, and S. Avril. A comprehensive study of layer-specific morphological changes in the microstructure of carotid arteries under uniaxial load. *Acta Biomater.* 57:342–351, 2017.

20. Lester, S. J., B. Heilbron, K. Gin, A. Dodek, and J. Jue. The natural history and rate of progression of aortic stenosis. , 1998.

21. Li, K., and W. Sun. Simulated Thin Pericardial Bioprosthetic Valve Leaflet Deformation Under Static Pressure-Only Loading Conditions: Implications for Percutaneous Valves. *Ann. Biomed. Eng.* 38:2690–2701, 2010.

22. Martin, C., and W. Sun. Simulation of long-term fatigue damage in bioprosthetic heart valves: effects of leaflet and stent elastic properties. *Biomech. Model. Mechanobiol.* 13:759–770, 2014.

23. Mirnajafi, A., J. Raymer, M. J. Scott, and M. S. Sacks. The effects of collagen fiber orientation on the flexural properties of pericardial heterograft biomaterials. *Biomaterials* 26:795–804, 2005.

24. Osnabrugge, R. L. J., D. Mylotte, S. J. Head, N. M. Van Mieghem, V. T. Nkomo, C. M. LeReun, A. J. J. C. Bogers, N. Piazza, and A. P. Kappetein. Aortic Stenosis in the Elderly. *J. Am. Coll. Cardiol.* 62:1002–1012, 2013.

25. Padala, M., E. L. Sarin, P. Willis, V. Babaliaros, P. Block, R. A. Guyton, and V. H. Thourani. An Engineering Review of Transcatheter Aortic Valve Technologies. *Cardiovasc. Eng. Technol.* 1:77–87, 2010.

26. Pasquino, E., S. Pascale, M. Andreon, S. Rinaldi, F. Laborde, and M. Galloni. Bovine pericardium for heart valve bioprostheses:in vitro andin vivo characterization of new chemical treatments. *J. Mater. Sci. Mater. Med.* 5:850–854, 1994.

27. Rotman, O. M., M. Bianchi, R. P. Ghosh, B. Kovarovic, and D. Bluestein. Principles of TAVR valve design, modelling, and testing. *Expert Rev. Med. Devices* 15:771–791, 2018.

28. Sacks, M. S., and C. J. Chuong. Orthotropic Mechanical Properties of Chemically Treated Bovine Pericardium. *Ann. Biomed. Eng.* 26:892–902, 1998.

29. Sacks, M. S., A. Mirnajafi, W. Sun, and P. Schmidt. Bioprosthetic heart valve heterograft biomaterials: structure, mechanical behavior and computational simulation. *Expert Rev. Med. Devices* 3:817–34, 2006.

30. Sacks, M. S., and F. J. Schoen. Collagen fiber disruption occurs independent of calcification in clinically explanted bioprosthetic heart valves. *J. Biomed. Mater. Res.* 62:359–371, 2002.

31. Sacks, M. S., and F. J. Schoen. Collagen fiber disruption occurs independent of calcification in clinically explanted bioprosthetic heart valves. *J. Biomed. Mater. Res.* 62:359–371, 2002.

32. Sacks, M. S., D. B. Smith, and E. D. Hiester. A Small Angle Light Scattering Device for Planar Connective Tissue Microstructural Analysis. *Ann. Biomed. Eng.* 25:678–589, 1997.

33. Sánchez-Arévalo, F. M., M. Farfán, D. Covarrubias, R. Zenit, and G. Pulos. The micromechanical behavior of lyophilized glutaraldehyde-treated bovine pericardium under uniaxial tension. *J. Mech. Behav. Biomed. Mater.* 3:640–646, 2010.

34. Schoen, F. J. Evolving concepts of cardiac valve dynamics: The continuum of development, functional structure, pathobiology, and tissue engineering. , 2008.

35. Schoen, F. J., J. Fernandez, L. Gonzalez-Lavin, and A. Cernaianu. Causes of failure and pathologic findings in surgically removed Ionescu- Shiley standard bovine pericardial heart valve bioprostheses: emphasis on progressive structural deterioration. *Circulation* 76:618–627, 1987.

36. Schultz, C. J., A. Weustink, N. Piazza, A. Otten, N. Mollet, G. Krestin, R. J. Van Geuns, P. De Feyter, † Patrick, W. J. Serruys, and P. De Jaegere. Geometry and Degree of Apposition of the CoreValve ReValving System With Multislice Computed Tomography After Implantation in Patients With Aortic Stenosis. , 2009.doi:10.1016/j.jacc.2009.04.075

37. Sellaro, T. L., D. Hildebrand, Q. Lu, N. Vyavahare, M. Scott, and M. S. Sacks. Effects of collagen fiber orientation on the response of biologically derived soft tissue biomaterials to cyclic loading. *J. Biomed. Mater. Res. - Part A* 80:194–205, 2007.

38. Siddiqui, R. F., J. R. Abraham, and J. Butany. Bioprosthetic heart valves: modes of failure. *Histopathology* 55:135–144, 2009.

39. Singhal, P., A. Luk, and J. Butany. Bioprosthetic Heart Valves: Impact of Implantation on Biomaterials. *ISRN Biomater.* 2013:1–14, 2013.

40. Smuts, A. N., D. C. Blaine, C. Scheffer, H. Weich, A. F. Doubell, and K. H. Dellimore. Application of finite element analysis to the design of tissue leaflets for a percutaneous aortic valve. *J. Mech. Behav. Biomed. Mater.* 4:85–98, 2011.

41. Sulejmani, F., A. Caballero, C. Martin, T. Pham, and W. Sun. Evaluation of transcatheter heart valve biomaterials: Computational modeling using bovine and porcine pericardium. *J. Mech. Behav. Biomed. Mater.* 97:159–170, 2019.

42. Sun, W., A. Abad, and M. S. Sacks. Simulated Bioprosthetic Heart Valve Deformation under Quasi-Static Loading. *J. Biomech. Eng.* 127:905, 2005.

43. Sun, W., K. Li, and E. Sirois. Simulated elliptical bioprosthetic valve deformation: Implications for asymmetric transcatheter valve deployment. *J. Biomech.* 43:3085–3090, 2010.

44. Sun, W., M. Sacks, G. Fulchiero, J. Lovekamp, N. Vyavahare, and M. Scott. Response of heterograft heart valve biomaterials to moderate cyclic loading. *J. Biomed. Mater. Res.* 69A:658–669, 2004.

45. Tremblay, D., T. Zigras, R. Cartier, L. Leduc, J. Butany, R. Mongrain, and R. L. Leask. A Comparison of Mechanical Properties of Materials Used in Aortic Arch Reconstruction. *Ann. Thorac. Surg.* 88:1484–1491, 2009.

46. Vesely, I., and D. Boughner. Analysis of the bending behaviour of porcine

xenograft leaflets and of natural aortic valve material: Bending stiffness, neutral axis and shear measurements. *J. Biomech.* 22:655–671, 1989.

47. Wells, S. M., T. Sellaro, and M. S. Sacks. Cyclic loading response of bioprosthetic heart valves: Effects of fixation stress state on the collagen fiber architecture. *Biomaterials* 26:2611–2619, 2005.

48. Whelan, A., J. Duffy, R. T. Gaul, D. O. Reilly, D. R. Nolan, P. Gunning, and C. Lally. Collagen fibre orientation and dispersion govern ultimate tensile strength , stiffness and the fatigue performance of bovine pericardium. *J. Mech. Behav. Biomed. Mater.* 90:54–60, 2019.

49. Zhang, W., and M. S. Sacks. Modeling the response of exogenously crosslinked tissue to cyclic loading: The effects of permanent set. *J. Mech. Behav. Biomed. Mater.* 75:336–350, 2017.

50. Zilla, P., J. Brink, P. Human, and D. Bezuidenhout. Prosthetic heart valves: Catering for the few. *Biomaterials* 29:385–406, 2008.

Appendix A:

Table A.1: Specimen parameters and cycles completed for uniaxial cyclic loading detailed in Section 3.2.

Sample #	Alignment	Angle (°)	Thickness (mm)	Cycles Completed	Alignment post-loading	Angle post-loading
XD1	0.728	83.218	0.329	1	N/A	N/A
XD2	0.702	81.27	0.371	126006	N/A	N/A
XD3	0.787	104.76	0.328	1000000	0.6806	103.95
XD4	0.7895	86.02	0.308	1	N/A	N/A
XD5	0.8069	76.4375	0.331	1	N/A	N/A
XD6	0.711	78.92	0.411	1	N/A	N/A
XD7	0.76009	80.416	0.439	22398	N/A	N/A
HD1	0.559	104.66	0.412	361737	N/A	N/A
HD2	0.567	13.63	0.394	493790	N/A	N/A
HD3	0.64	93	0.336	327147	N/A	N/A
HD4	0.56114	37.927	0.412	1000000	0.594	19.95
HD5	0.571	82.02	0.408	1000000	0.644	-21.47
HD6	0.584	-23.57	0.401	1000000	0.6706	-11.04
HD7	0.613	-17	0.370	1000000	Not possible	Not possible
PD1	0.73	-6.9	0.399	1000000	0.768	0.4062
PD2	0.725	2.85	0.400	1000000	0.741	0.458
PD3	0.807	-0.645	0.335	1000000	0.839	-4.48
PD4	0.784	13.59	0.366	1000000	0.8325	3.41
PD5	0.727	-3.02	0.350	1000000	0.7886	-0.95
PD6	0.8159	4.645	0.319	1000000	0.81655	4.375
PD7	0.76059	-1.5	0.330	1000000	0.7979	-2.34

N/A: SALS was not possible after loading due to sample failure. N/A* for sample HD7: SALS imaging was not possible due to mishandling of the specimen, resulting in increased opacity.

Table A.2: Mean collagen fibre angle and alignment values for interrogation regions on GLBP patch (n=24)

Sample	Angle (°)	Alignment	Sample	Angle (°)	Alignment
a	74.16	0.74	m	63.50	0.80
b	37.52	0.69	n	63.71	0.77
c	37.46	0.69	o	63.67	0.74
d	54.55	0.70	p	72.83	0.66
e	68.82	0.74	q	80.04	0.72
f	65.70	0.74	r	81.01	0.71
g	74.11	0.66	s	53.52	0.70
h	80.70	0.60	t	56.7	0.79
i	91.46	0.76	u	53.42	0.78
j	75.70	0.70	v	54.24	0.74
k	62.06	0.70	w	51.28	0.70
l	58.16	0.81	x	57.87	0.61

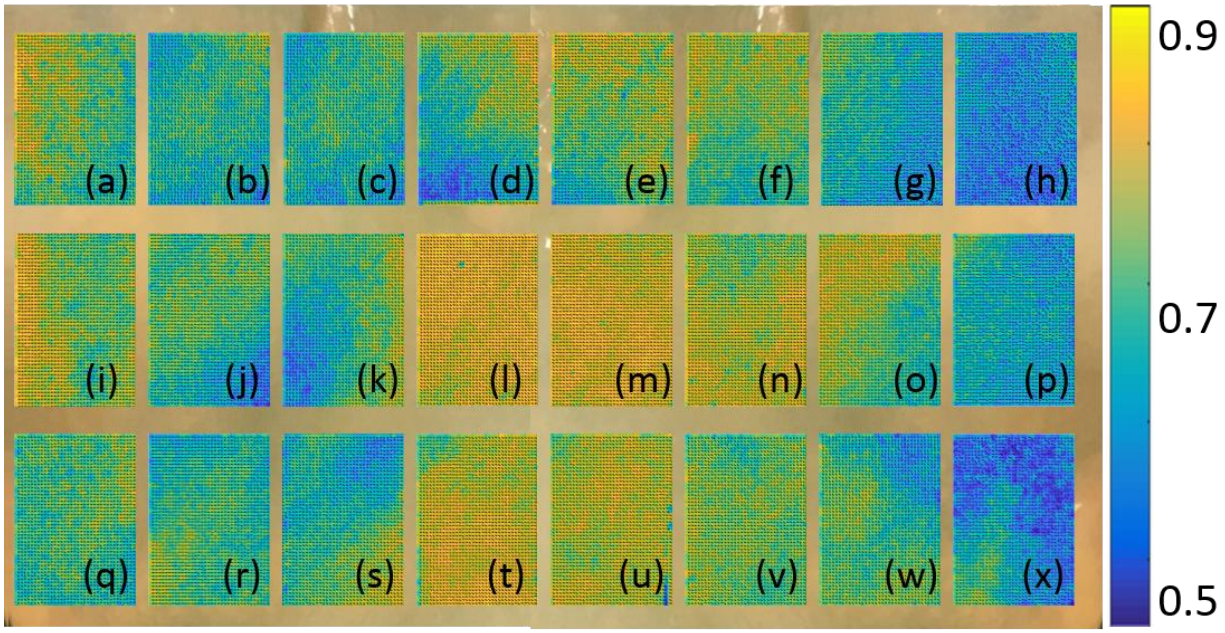

Figure A.1: *SALS analysis overlaid on full GLBP patch. Interrogation region labelling (a-x) correspond to fibre architecture detailed in Table A.2 above.*

Supplementary Material:

Table S.1: Specimen parameters for uniaxial monotonic loading detailed in Section 4

Sample	Angle	Alignment	UTS (MPa)	Stiffness (MPa)
XD1	79.31	0.80	1.43	26.92
XD2	82.63	0.77	3.41	25.88
XD3	82.17	0.76	3.69	27.17
XD4	77.46	0.74	3.42	27.03
XD5	78.96	0.77	1.46	25.47
XD6	99.96	0.72	2.67	33.59
HD1	N/A	0.50	13.91	103.04
HD2	N/A	0.55	31.83	222.14
HD3	N/A	0.62	22.95	193.92
HD4	N/A	0.54	9.48	75.46
HD5	N/A	0.62	5.90	49.16
HD6	N/A	0.5	7.49	96.03
PD1	-3.67	0.72	25.50	152.85
PD2	-7.15	0.75	27.66	209.02
PD3	-15.27	0.79	17.09	149.52
PD4	-2.98	0.80	18.69	183.31
PD5	5.38	0.80	19.57	191.43
PD6	4.46	0.80	18.64	173.21

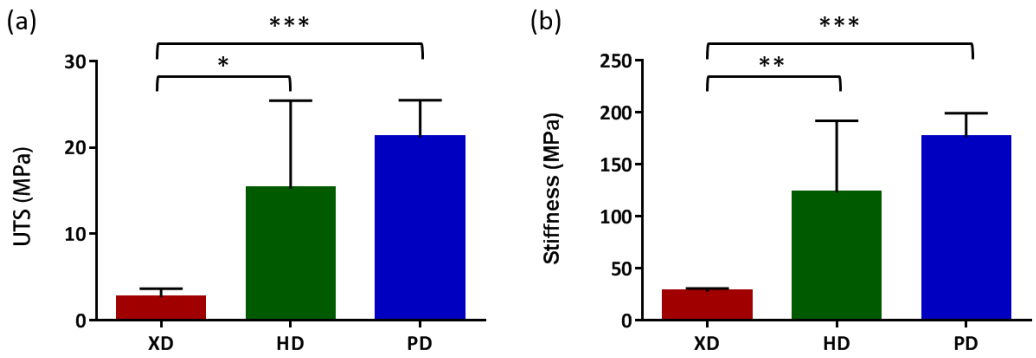

Figure S.1: *(a) UTS of XD, HD and PD specimens where *p < 0.05, ***p<0.001. (b) Stiffness values of XD, HD and PD specimens, where **p<0.01, ***p < 0.001.*

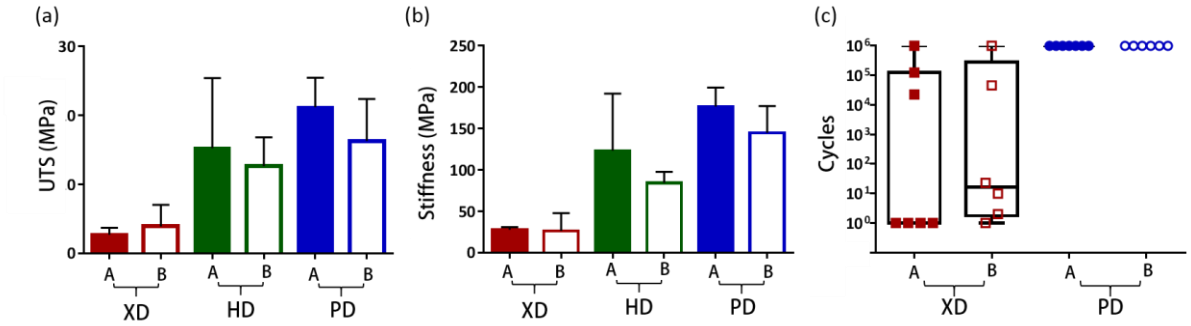

Figure S.2: *Type 'A' is the GLBP tested in this study, and Type 'B' is the GLBP tested in our previous work (Whelan et al., 2019).* ***(****a) UTS values for XD, HD and PD specimen groups for Type A and Type B tissue. (b) Cycles completed for XD and PD specimen groups for Type A and Type B tissue. (Note: t-test analyses were conducted between the two tissue types, for each specimen group; XD, HD and PD).*